Academic Journal of Science and Technology
ISSN: 2771-3032 | Vol. 21, No. 2, 2026

Characteristics of Greenhouse Gas Emission Factors in Sewer Networks, Key Influencing Factors, and Responses to Network Defects

Zixin Chen[1, *]

[1]College of Environmental Science and Engineering, Tongji University, Shanghai, 200092, China

[*] Corresponding author

Abstract: Drainage networks, long treated as passive conduits, are now recognized as GHG sources, yet controls on their emission factors (EFs) remain unclear. We synthesized 138 EFs (111 CH_4, 27 N_2O) from 24 studies (1994–2024), deploying Spearman, Random-Forest-SHAP, and GAMs to pinpoint drivers and nonlinear responses, alongside defect scenarios mimicking illicit flows and rainfall intrusion. Pressurized mains exhibited the highest dissolved CH_4, whereas N_2O partitioned predominantly into the dissolved phase across systems. CH_4 EFs responded chiefly to hydraulics and organics (A/V ratio, COD, depth, temperature), while N_2O EFs shifted toward nitrogen pathways (NH_4^+-N, NO_3^--N, conductivity). Simulations revealed opposing trends: defect severity suppressed CH_4 but elevated N_2O, with rainfall amplifying this divergence. These findings argue against static EFs—emission factors are context-sensitive, varying with hydraulics, chemistry, and pipe integrity. Incorporating such dynamic dependencies would sharpen urban GHG inventories and targeted abatement strategies.

Keywords: Drainage network; Greenhouse gas; Emission factor; Methane; Nitrous oxide; Sewer defects.

1. Introduction

Global warming concerns have increasingly centered on CH_4 and N_2O—whose 100-year warming potentials are 27 and 273 times that of CO_2, respectively [1]. Urban water systems emit these gases, yet drainage networks are still widely regarded as passive conduits rather than reactive sources [2]. Emerging evidence, however, portrays sewers as biochemical reactors where organic matter decay and nitrogen conversions produce substantial CH_4 and N_2O [3]. Such production intensifies under pressurized or oxygen-limited conditions [4], though reported EFs vary greatly across studies due to differences in measurement protocols and local environments [5].

Despite the widespread use of EFs in GHG accounting [6], critical knowledge gaps persist: (i) no systematic EF comparison exists between pressurized and gravity sewers; (ii) combined effects of hydraulic and water-quality factors remain unclear; and (iii) static EFs fail to account for sewer defects—illicit connections, leaks, and rainfall intrusions—that are common in practice. China's sewer network had surpassed 1 million km by 2023 [7], making it urgent to understand EF variability and defect-induced responses for reliable emission estimates.

To address these gaps, we assembled 138 EF records from 1994–2024, compared conveyance modes and occurrence phases, identified key drivers via Spearman correlation, Random-Forest-SHAP, and GAMs, and simulated defect severity alongside rainfall impacts. We further explore the implications of adopting dynamic, context-sensitive EFs over fixed values for urban drainage GHG inventories.

2. Materials and Methods

2.1. Data acquisition

To build the GHG emission factor database, we systematically searched the Web of Science Core Collection [8,9] for studies published from 1994 through 2024, using the query: TS = ("nitrous oxide" OR "methane" OR "carbon dioxide" OR "greenhouse gas") AND TS = ("sewer" OR "drainage network" OR "sewerage systems").

We applied five inclusion criteria: (i) the system studied had to be a drainage or sewage conveyance network; (ii) CH_4 or N_2O concentrations, fluxes, or EFs had to be reported; (iii) both conveyance mode and occurrence phase had to be identifiable; (iv) hydraulic, water-quality, or environmental data had to accompany the EF records; and (v) monitoring protocols and data sources had to be clearly documented. We excluded duplicates, incomplete records, and papers without extractable numerical data. Since CO_2 data proved too sparse for robust comparison, we restricted our analyses to CH_4 and N_2O.

This screening yielded 24 eligible studies, from which we compiled 138 EF records: 111 for CH_4 (32 dissolved from pressurized sewers, 38 gaseous from gravity sewers, and 41 dissolved from gravity sewers) and 27 for N_2O (12 gaseous and 15 dissolved, both from gravity sewers). For each record, we extracted eleven environmental covariates—temperature, pH, COD, NH_4^+-N, NO_3^--N, conductivity, flow velocity, water depth, hydraulic retention time, pipe diameter, and A/V ratio.

For subsequent analyses, we sorted the EFs into five categories defined by the combination of conveyance mode and occurrence phase: dissolved CH_4 in pressurized mains, dissolved CH_4 in gravity lines, gaseous CH_4 in gravity lines, dissolved N_2O in gravity lines, and gaseous N_2O in gravity lines. Each category was then analyzed separately for EF characterization, driver identification, and defect-scenario simulation.

2.2. Characteristic analysis and control mechanism identification of emission factors

We visualized EF distributions across conveyance modes

and occurrence phases via violin-boxplot combinations, with non-parametric tests further assessing inter-category differences. Spearman rank correlation served to screen pairwise relationships between EFs and environmental covariates. To disentangle variable contributions, we trained a random forest model, interpreting its outputs through the SHAP (Shapley Additive Explanations) framework [10], with importance ranked by mean absolute SHAP values. The top predictors identified from this step were then fed into generalized additive models (GAMs) to delineate nonlinear response shapes and locate potential thresholds [11].

2.3. Scenario construction and response analysis for sewer defects

To assess how sewer defects reshape GHG emission factors, we designed three defect scenarios grounded in typical abnormal sewage transport pathways found in urban drainage systems. Scenario P0 represents normal operation, with sewage conveyed through sewers under standard conditions. Scenario P1 captures illicit connections or misconnections that divert sewage into stormwater pipes. Scenario P2 goes a step further—sewage that has entered the stormwater network then mixes with rainfall runoff. Taken together, this sequence (P0 → P1 → P2) traces a gradient from intact to increasingly defect-compromised transport.

At the system level, we used the sewage centralized collection rate as a proxy for abnormal transport intensity. Lower collection rates signify greater sewage loss and stronger perturbations from illicit inflows, allowing us to represent different defect severities. For the P2 scenario specifically, we adopted stormwater pipe fullness (h/D) as an indicator of rainfall intensity, and examined how EFs shift across varying fullness levels to untangle the joint effects of rainfall and defects on GHG emissions. All statistical computations and data handling were performed in R.

3. Results and discussion

3.1. Characteristic differences in GHG emission factors from drainage networks

Figure 1 reveals marked variability in CH_4 and N_2O EFs across conveyance modes and phases. Both gases showed significant phase-dependent differences ($P < 0.001$), yet their dominant occurrence forms diverged sharply.

For CH_4, dissolved EFs in pressurized mains significantly exceeded those in gravity sewers ($P < 0.001$) [12], and also surpassed gaseous EFs from gravity systems. Pressurized dissolved CH_4 averaged 9.11 mg L^{-1} (maximum: 32.14 mg L^{-1}), with wide scatter. By contrast, gravity dissolved CH_4 averaged only 0.30 mg L^{-1}, while gravity gaseous CH_4 reached 6.65 mg L^{-1}—roughly 22 times its dissolved counterpart in the same systems. This stark partitioning likely stems from hydraulic contrasts: pressurized pipes are enclosed, oxygen-depleted, and retention-prone, favoring sustained methanogenesis and liquid-phase CH_4 buildup [13]; gravity lines, conversely, feature drop structures, turbulence, and interfacial disturbance, driving dissolved CH_4 toward continuous degassing and elevating gaseous EFs.

N_2O displayed the opposite trend. In gravity systems, dissolved N_2O averaged 9.79 μg L^{-1} versus only 0.058 μg L^{-1} for gaseous N_2O—a nearly 170-fold difference [14]. Gaseous N_2O remained uniformly low across all records, whereas dissolved values spanned 3.9–26 μg L^{-1}, indicating substantial variability.

Unlike CH_4's pronounced gas–liquid partitioning, N_2O accumulates preferentially in the dissolved phase. This divergence likely reflects their distinct biogeochemical origins: N_2O production ties to nitrification–denitrification pathways, modulated by dissolved O_2, nitrogen species, and redox potential, with a portion of produced N_2O further reduced to N_2 before outgassing—restraining its gaseous escape.

CH_4 and N_2O thus operate through fundamentally different mechanisms in sewer networks. CH_4 distribution hinges on anaerobic production plus physical stripping, with conveyance mode dictating phase preference; N_2O instead tracks the intensity of nitrogen conversions, remaining largely in solution rather than volatilizing. These contrasts argue strongly against single-phase or uniform EFs for drainage networks. Of particular concern are the large dissolved CH_4 pools in pressurized mains and dissolved N_2O stocks in gravity sewers—both represent latent emissions that may be released downstream during treatment or transport, meriting closer scrutiny in future work.

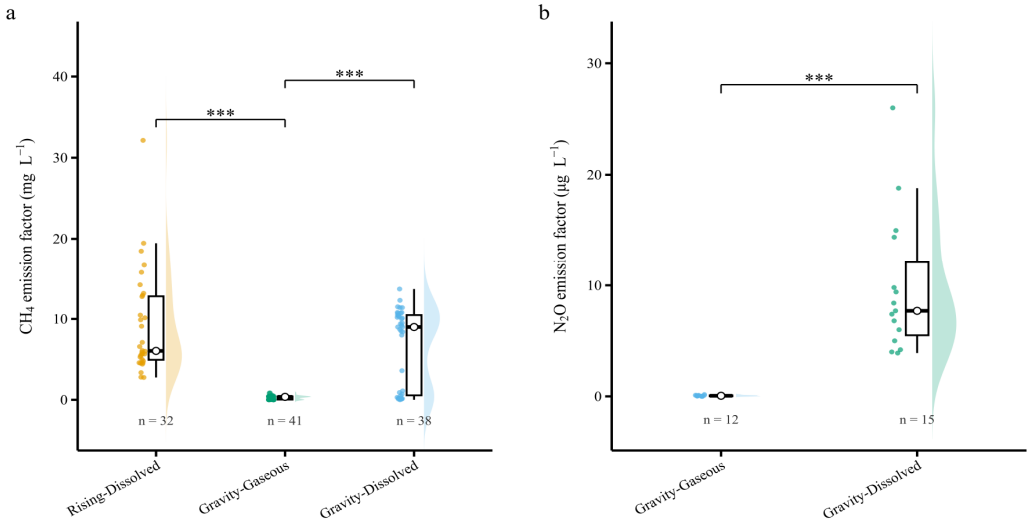

Figure 1. Distribution characteristics of CH_4 and N_2O emission factors under different sewer transport modes and occurrence phases.(a) CH_4 emission factors; (b) N_2O emission factors. Dots represent individual observations, violin plots indicate data density distributions, boxplots show the median and interquartile range (IQR), and white circles represent mean values. Asterisks (***) indicate statistically significant differences between groups ($P < 0.001$).

3.2. Control mechanisms of GHG emission factors in drainage networks

3.2.1. Identification of key influencing factors

Figure 2 illustrates that while EF controls differ markedly across conveyance modes and phases, they collectively reflect hydraulic, water-quality, and environmental drivers—yet with distinct emphases for each gas.

For CH_4 in pressurized mains, dissolved EFs correlated positively with pipe diameter, A/V ratio, and flow velocity, but negatively with pH—consistent with the notion that enclosed, anaerobic conditions favor methanogenesis and liquid-phase retention. In gravity sewers, both dissolved and gaseous CH_4 EFs tracked positively with HRT, COD, temperature, and water depth [15,16], aligning with the expectation that prolonged retention and abundant organics stimulate methanogenic activity.

N_2O told a different story. Dissolved N_2O EFs correlated positively with NH_4^+-N, NO_3^--N, and pH, while showing a weak negative temperature dependence [17]. Gaseous N_2O, in turn, responded positively to temperature, COD, and pH, but negatively to water depth and conductivity. These patterns implicate nitrogen-transformation pathways—nitrification and denitrification—as the primary N_2O source, with gas–liquid exchange playing a secondary modulating role.

In essence, CH_4 EFs are hydraulics- and organics-driven, whereas N_2O EFs are nitrogen-cycle-dominated—pointing to fundamentally distinct formation mechanisms. We further applied machine learning to help pinpoint potential key drivers beyond these bivariate associations.

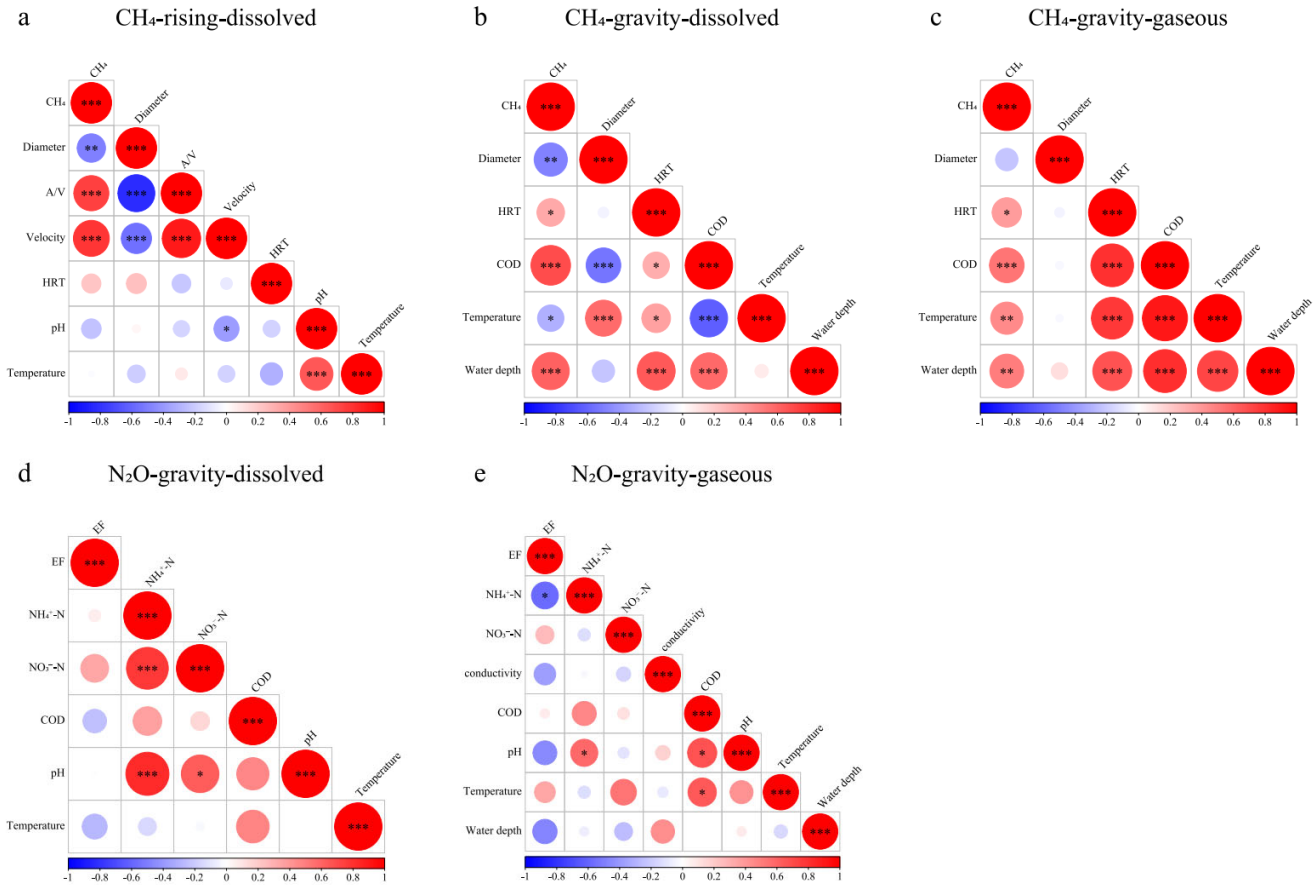

Figure 2. Spearman correlation analysis between GHG emission factors and environmental factors under different conveyance modes and occurrence phases. (a) CH_4-pressurized-dissolved; (b) CH_4-gravity -dissolved; (c) CH_4-gravity-gaseous; (d) N_2O-gravity-dissolved; (e) N_2O-gravity-gaseous. Circle color indicates the magnitude and direction of the correlation coefficient: red represents positive correlation, blue represents negative correlation. Circle size indicates the strength of the correlation. *, **, and *** denote significance at $P < 0.05$, $P < 0.01$, and $P < 0.001$ levels, respectively.

3.2.2. Importance analysis of key influencing factors

To rank driver importance, we employed random forest with SHAP (Figure 3). Dominant controls varied markedly by gas species and phase.

For pressurized dissolved CH_4 (Figure 3a), A/V ranked first, with pipe diameter, flow velocity, and HRT following in descending order [18]—highlighting structural and hydraulic constraints on CH_4 buildup. In gravity sewers, dissolved CH_4 EFs (Figure 3b) were most strongly driven by water depth and COD, while gaseous CH_4 (Figure 3c) responded chiefly to COD, temperature, and water depth [19]. Substrate supply, ambient conditions, and gas–liquid exchange thus collectively shape CH_4 emissions.

N_2O EFs followed a distinctly nitrogen-oriented pattern. For dissolved N_2O (Figure 3d), COD, NO_3^--N, and NH_4^+-N dominated predictions; for gaseous N_2O (Figure 3e), electrical conductivity and NH_4^+-N led, with water depth and pH secondary [20].

In short, CH_4 EFs are governed primarily by hydraulics and organics, whereas N_2O EFs are regulated by nitrogen-cycle parameters—confirming that the two GHGs arise via fundamentally distinct mechanisms, which sets the stage for exploring their nonlinear responses to key drivers.

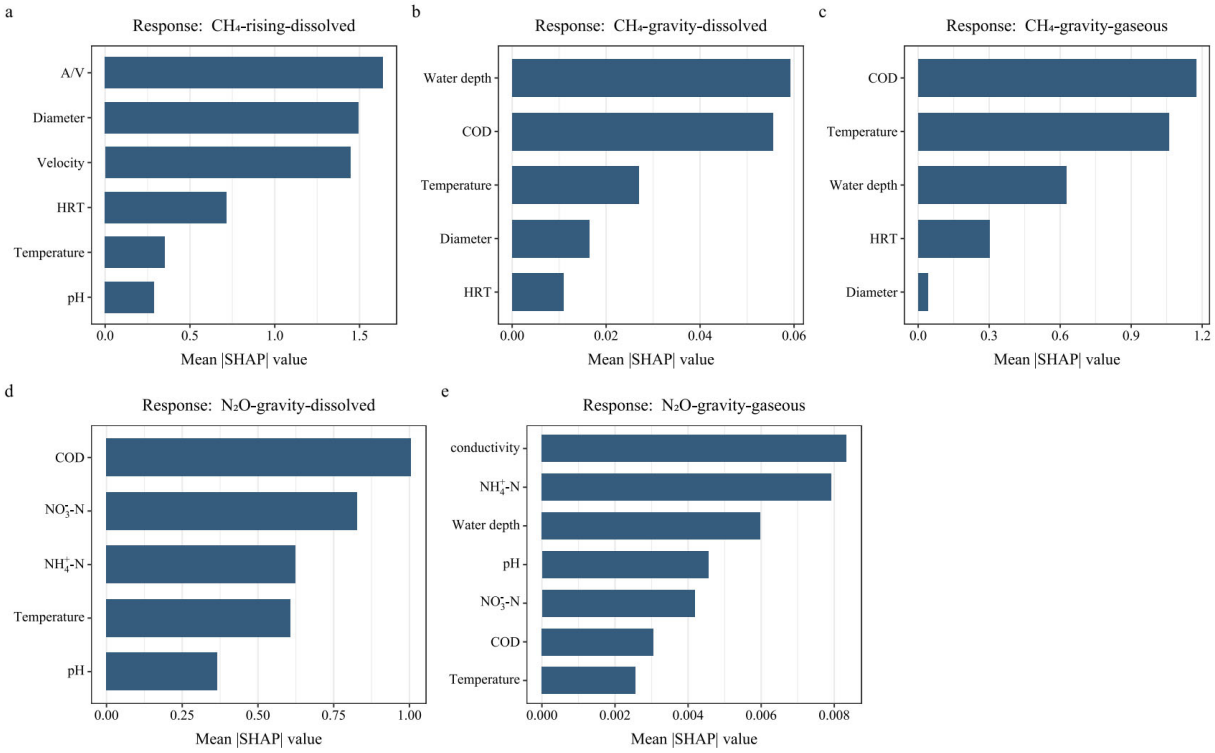

Figure 3. Random Forest–SHAP importance rankings of key drivers for each EF category. Panels (a)–(e) correspond to: (a) CH_4–pressurized–dissolved; (b) CH_4–gravity–dissolved; (c) CH_4–gravity–gaseous; (d) N_2O–gravity–dissolved; (e) N_2O–gravity–gaseous. The x-axis denotes the mean absolute SHAP value—larger values signify greater contributions to model predictions.

3.2.3. Response patterns of emission factors to key factors

To probe how key drivers shape GHG EFs beyond linear associations, we fitted generalized additive models (GAMs) to the SHAP-identified predictors (Figure 4). Nonlinear responses with multiple thresholds emerged across all EF categories.

For pressurized dissolved CH_4 (Figure 4a–c), A/V ratio, pipe diameter, and flow velocity each exhibited clear breakpoints. Notably, A/V near 20 m^{-1} and flow velocity around 1.3 m s^{-1} marked sharp turning points [21], beyond which the positive effects on CH_4 EFs intensified markedly. In gravity sewers, dissolved CH_4 (Figure 4d–f) showed persistently positive responses to water depth and COD, with acceleration near 0.5 m and 121 mg L^{-1}, respectively [22]; temperature, however, followed a more intricate nonlinear path. For gaseous CH_4 (Figure 4g–i), COD, water depth, and temperature all tracked positively with model predictions—temperature notably exhibited a U-shaped pattern, with stronger enhancement at higher thermal levels [23].

N_2O responses diverged. For dissolved N_2O (Figure 4j–l), NO_3^--N exhibited a threshold near 0.8 mg L^{-1}, whereas NH_4^+-N followed a unimodal (single-peak) trajectory [24]. For gaseous N_2O (Figure 4m–o), NH_4^+-N, conductivity, and water depth all showed threshold-like inflections—NH_4^+-N transitioned sharply around 21 mg L^{-1}, while rising conductivity generally suppressed model responses.

Collectively, these response shapes reinforce that CH_4 EFs couple closely with hydraulics, organics, and temperature, whereas N_2O EFs pivot primarily on nitrogen transformations. The diversity of threshold, U-shaped, and unimodal patterns underscores the complex regulation of GHG EFs in sewers, lending strong support for adopting dynamic, context-sensitive EF frameworks over static alternatives.

3.3. Impact of sewer defects on GHG emission factors

3.3.1. Scenario construction based on abnormal sewage transport processes

Sewer defects can alter hydraulic conditions and sewage routing, with potential consequences for GHG emissions. To investigate this, we established a scenario framework (Table 1) representing three progressively compromised transport states observed in urban drainage systems.

Scenario P0 served as the reference—sewage conveyed through sewers under normal operation. Scenario P1 describes sewage diverted into stormwater pipes via illicit connections or misconnections. Scenario P2 represents a further stage: sewage that has entered the stormwater network then mixes with incoming rainfall runoff. As the transition from P0 to P2 proceeds, the flow path, hydraulic regime, and water chemistry all shift, potentially modifying EF behavior [25].

This progression—"normal transport (P0) → abnormal inflow (P1) → mixed transport (P2)"—thus captures a gradient from intact to defect-affected sewer conditions, providing the basis for evaluating EF responses across different defect severities.

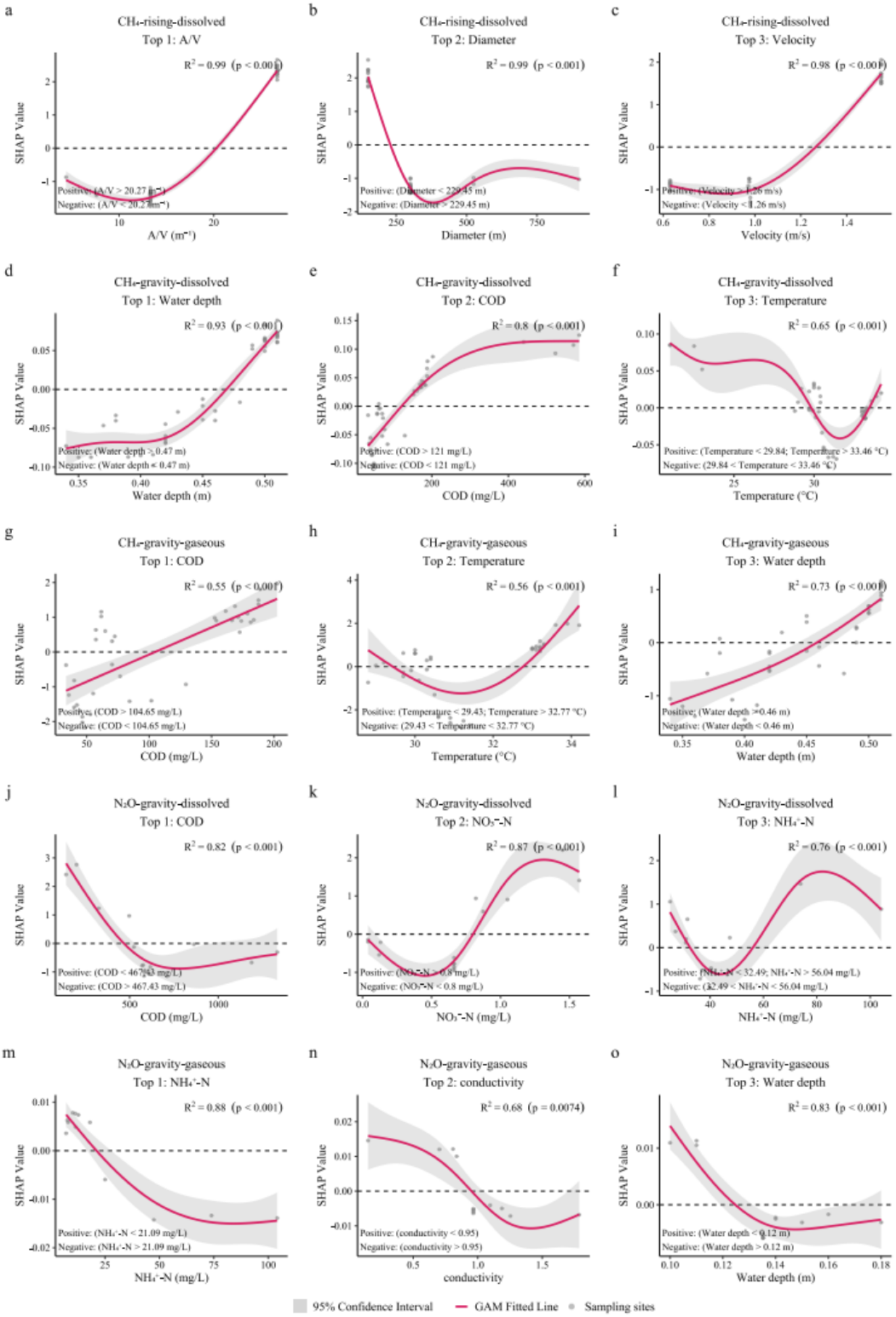

Figure 4. GAM-derived response curves relating GHG EFs to key SHAP-identified drivers. Panels (a–c): CH_4–pressurized–dissolved; (d–f): CH_4–gravity–dissolved; (g–i): CH_4–gravity–gaseous; (j–l): N_2O–gravity–dissolved; (m–o): N_2O–gravity–gaseous. The red line shows the GAM fit, with the gray band denoting the 95% confidence interval and individual measurements plotted as gray dots. The x-axis gives the driver value; the y-axis gives the corresponding SHAP value.

Table 1. Definition of defect path scenarios

Scenario ID	Path name	Corresponding defect	Main process	Application scenario
P0	Normal transport	—	—	Sewer pipe
P1	Abnormal inflow	Illicit connection / misconnection	Sewage enters stormwater pipe	Stormwater pipe
P2	Mixed transport	Combined sewer-stormwater	Sewage mixed with rainfall runoff	Stormwater pipe

3.3.2. Response characteristics of emission factors to defect severity

Using the scenario framework from Section 3.3.1, we employed the sewage centralized collection rate as a proxy for defect severity and traced how GHG EFs responded across scenarios (Figure 5). The responses were strongly gas- and phase-specific.

For CH_4 (Figure 5a–c), pressurized dissolved EFs under both P1 and P2 fell below the P0 baseline, converging toward it as the collection rate increased [26]. In gravity sewers, dissolved CH_4 under P1 dropped below P0, yet P2 consistently exceeded the baseline. Gaseous CH_4, however, remained below P0 under both P1 and P2, with the gap widening as defects intensified.

N_2O followed a contrasting trajectory (Figure 5d–e). Dissolved N_2O under P1 was lower than P0, but under P2 it rose above the baseline. Gaseous N_2O under both defect scenarios surpassed P0, with P1 recording the highest levels [27].

In brief, CH_4 and N_2O responded in opposite directions to increasing defect severity: CH_4 EFs generally declined, whereas N_2O EFs trended upward under the abnormal inflow and mixed-transport conditions examined here. These divergent responses confirm that sewage transport disturbances can profoundly reshape GHG emission profiles in drainage networks, with distinct implications for each gas.

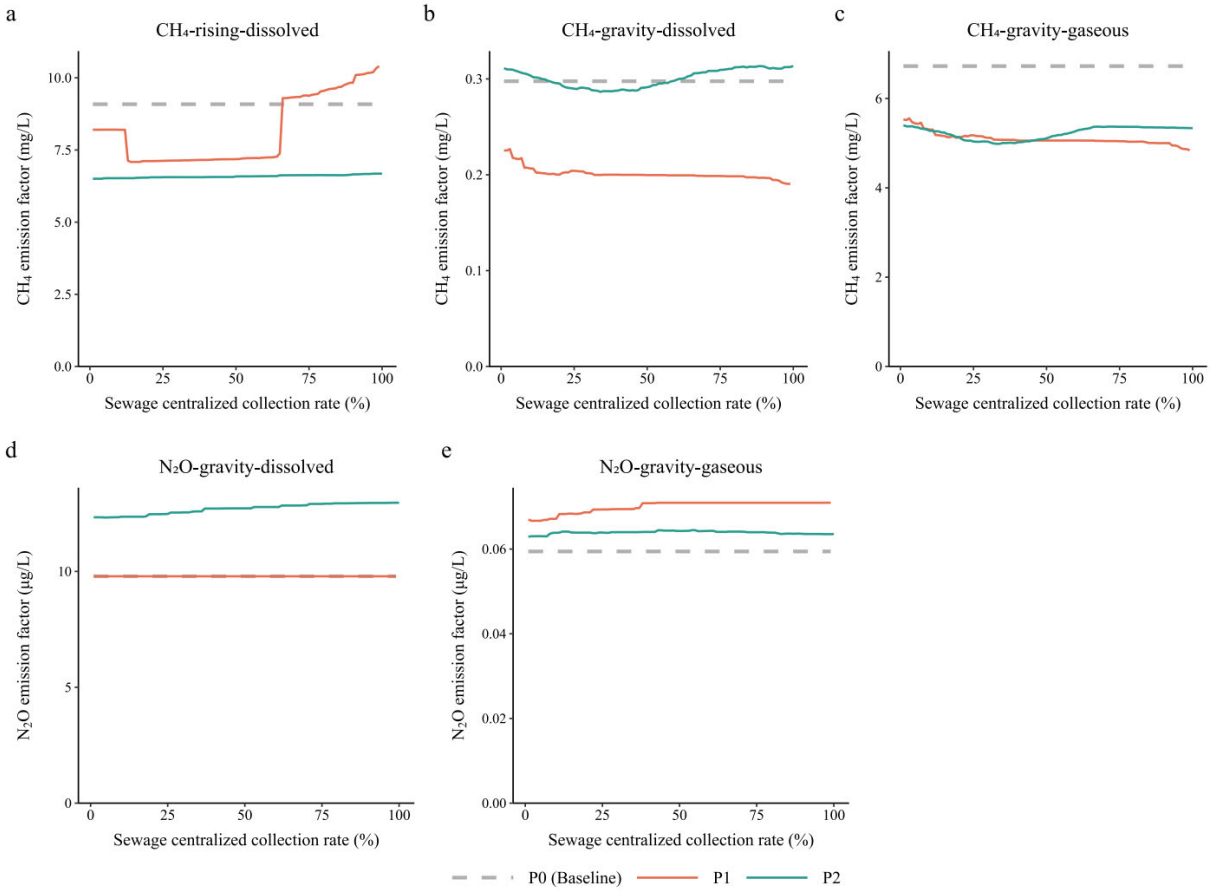

Figure 5. GHG emission factor responses to sewage centralized collection rate across defect scenarios. Panels (a)–(e) correspond to: (a) CH_4–pressurized–dissolved; (b) CH_4–gravity–dissolved; (c) CH_4–gravity–gaseous; (d) N_2O–gravity–dissolved; (e) N_2O–gravity–gaseous. The x-axis denotes the centralized collection rate (a proxy for defect severity); the y-axis gives the corresponding EF value. The gray dashed line marks the P0 (normal transport) baseline; the red and green solid lines represent P1 (abnormal inflow) and P2 (mixed transport with rainfall), respectively.

4. Conclusions and implications

Based on 24 peer-reviewed studies (1994–2024), we compiled a GHG emission factor database for drainage networks with 138 records, and systematically examined EF variations, controlling drivers, and responses to sewer defects. The key findings are as follows:

(1) EFs vary markedly by gas species, conveyance mode, and occurrence phase. Pressurized mains yield the highest dissolved CH_4 EFs. In gravity sewers, CH_4 partitions predominantly into the gas phase, whereas N_2O remains largely dissolved—with dissolved N_2O EFs far exceeding their gaseous counterparts. A single, lump-sum EF thus poorly represents the actual emission landscape of drainage networks.

(2) CH_4 and N_2O EFs are governed by fundamentally different drivers. CH_4 responds primarily to hydraulic conditions and organic substrate availability—A/V ratio, COD, water depth, and temperature rank as the top contributors. N_2O EFs, by contrast, are tightly coupled to nitrogen transformation pathways, particularly NH_4^+-N, NO_3^--N, and electrical conductivity [28]. Many of these relationships exhibit nonlinear or threshold-type behavior.

(3) Sewer defects exert a significant and divergent influence: under illicit inflow and stormwater-mixing scenarios, CH_4 EFs tend to decrease while N_2O EFs rise—a

contrast further amplified by rainfall.

Overall, our findings argue against static EFs for drainage networks. EF variability reflects the intertwined effects of transport conditions, environmental settings, and infrastructure integrity. Embedding these dynamic influences into EF estimation would enhance the reliability of urban GHG inventories and support more informed mitigation assessments.

5. Uncertainty analysis

Several uncertainties warrant mention despite our relatively comprehensive dataset. The analysis draws on only 24 studies, with limited sample sizes for some EF categories—particularly N_2O. Heterogeneity in monitoring protocols, sampling designs, and site conditions across studies may also propagate into EF estimates. Moreover, our defect scenarios, while grounded in representative abnormal transport pathways, inevitably simplify real-world complexity—leakage, sediment buildup, and network heterogeneity are not explicitly represented.

Future work could strengthen EF characterizations by integrating long-term field observations with digital twin technologies to construct spatiotemporally explicit models [29]. Such approaches would better resolve emission dynamics and reduce accounting uncertainties for drainage network GHGs.

References

[1] IPCC. (2021). Climate Change 2021: The Physical Science Basis. Contribution of Working Group I to the Sixth Assessment Report of the Intergovernmental Panel on Climate Change. Cambridge University Press.

[2] Wang, Y., Zhang, L., & Li, H. (2025). Carbon emission characteristics and reduction technologies in urban wastewater systems: A review. *Water Cycle*, 6, 285–299.

[3] Foley, J., Yuan, Z., & Lant, P. (2009). Dissolved methane in rising main sewer systems: Field measurements and simple model development for estimating greenhouse gas emissions. *Water Science and Technology*, 60(11), 2963–2971. https://doi.org/10.2166/wst.2009.693

[4] Sharma, K., Li, J., Liu, T., Willis, J., Liu, Y., Zhang, Z., & Yuan, Z. (2026). Estimating methane emissions from global sewer networks. *Nature Water*, 4(2), 196–205. https://doi.org/10.1038/s44221-026-00032-7

[5] IPCC. (2006). 2006 IPCC Guidelines for National Greenhouse Gas Inventories, Volume 5: Waste. IPCC National Greenhouse Gas Inventories Programme.

[6] Chen, X., & Wang, J. (2024). Methane production mechanism and control strategies for sewers: A critical review. *Water*, 16(24), 3621. https://doi.org/10.3390/w16243621

[7] Li, M., Zhao, Y., & Zhou, X. (2024). Research progress on monitoring methods of direct carbon emissions from urban sewage collecting systems. *Environmental Engineering*, 42(11), 13–21.

[8] IPCC. (2019). 2019 Refinement to the 2006 IPCC Guidelines for National Greenhouse Gas Inventories. IPCC.

[9] Yuan, Z., Ni, B. J., & Van Loosdrecht, M. C. M. (2026). The biogeochemical origin of sewage gases and control of their generation. *Water Research*, 210, 118–130. https://doi.org/10.1016/j.watres.2026.118130

[10] Rocher-Ros, G., Stanley, E. H., Loken, L. C., Casson, N. J., Raymond, P. A., Liu, S., … Humborg, C. (2023). Global methane emissions from rivers and streams. *Nature*, 621(7979), 530–535. https://doi.org/10.1038/s41586-023-06408-7

[11] Liu, Y., Ni, B. J., & Yuan, Z. (2025). Assessment of methane and nitrous oxide emissions from urban community sewer networks: Field quantification and insights into environmental factors. *Journal of Environmental Management*, 373, 123456. https://doi.org/10.1016/j.jenvman.2025.123456

[12] Guisasola, A., de Haas, D., Keller, J., & Yuan, Z. (2008). Methane formation in sewer systems. *Water Research*, 42(6–7), 1421–1430. https://doi.org/10.1016/j.watres.2007.10.034

[13] Zhang, H., Feng, C., & Zhou, X. (2025). Impact of digitization and artificial intelligence on carbon emissions considering variable interaction and heterogeneity: An interpretable deep learning modeling framework. *Sustainable Cities and Society*, 109, 105678. https://doi.org/10.1016/j.scs.2025.105678

[14] Wang, L., Chen, D., & Liu, S. (2024). Intelligent management of carbon emissions of urban domestic sewage based on the Internet of Things. *Environmental Research*, 246, 118025. https://doi.org/10.1016/j.envres.2024.118025

[15] Mannina, G., Cosenza, A., & Van Loosdrecht, M. C. M. (2022). Greenhouse gases emission from wastewater treatment plants: A review of measurement methods. *Science of the Total Environment*, 828, 154372. https://doi.org/10.1016/j.scitotenv.2022.154372

[16] Short, M. D., Daikeler, A., Wallis, K., Peirson, W. L., & Peters, G. M. (2017). Dissolved methane in the influent of three Australian wastewater treatment plants fed by gravity sewers. *Science of the Total Environment*, 599–600, 85–93. https://doi.org/10.1016/j.scitotenv.2017.04.190

[17] Foley, J., Yuan, Z., & Lant, P. (2009). Development of a model for assessing methane formation in rising main sewers. *Water Research*, 43(11), 2874–2884. https://doi.org/10.1016/j.watres.2009.03.033

[18] Daelman, M. R. J., Van Loosdrecht, M. C. M., & Volcke, E. I. P. (2026). Methane emission from sewers. *Nature Water*, 4, 118–125. https://doi.org/10.1038/s44221-026-00028-3

[19] Daelman, M. R. J., van Voorthuizen, E. M., van Dongen, U. G. J. M., Volcke, E. I. P., & van Loosdrecht, M. C. M. (2022). Full-scale emission results (N_2O and CH_4) from wastewater treatment plants and sewer networks. *Water Research*, 210, 118–130. https://doi.org/10.1016/j.watres.2022.118130

[20] Jiang, G., Gutierrez, O., Sharma, K. R., & Yuan, Z. (2013). Effects of nitrate dosing on methanogenic activity in a sulfide-producing sewer biofilm reactor. *Water Research*, 47(5), 1788–1799. https://doi.org/10.1016/j.watres.2012.12.052

[21] Foley, J., Yuan, Z., & Lant, P. (2009). Development of a model for assessing methane formation in rising main sewers. *Water Research*, 43(11), 2874–2884. https://doi.org/10.1016/j.watres.2009.03.033

[22] Short, M. D., Daikeler, A., Wallis, K., Peirson, W. L., & Peters, G. M. (2017). Dissolved methane in the influent of three Australian wastewater treatment plants fed by gravity sewers. *Science of the Total Environment*, 599–600, 85–93. https://doi.org/10.1016/j.scitotenv.2017.04.190

[23] Chen, X., Jiang, G., & Yuan, Z. (2024). Methane mitigation via the nitrite-DAMO process induced by nitrate dosing in sewers. *Environmental Science & Technology*, 58(15), 6789–6798. https://doi.org/10.1021/acs.est.4c00321

[24] Liu, Y., Ni, B. J., & Yuan, Z. (2025). Assessment of methane and nitrous oxide emissions from urban community sewer networks: Field quantification and insights into environmental factors. *Journal of Environmental Management*, 373, 123456. https://doi.org/10.1016/j.jenvman.2025.123456

[25] Monje, V., Petit, S., & Maier, M. (2025). Inflows into wastewater systems and the water-energy-greenhouse gases

emissions nexus: Opportunities and challenges for asset management. *Water Research*, 245, 120567. https://doi.org/10.1016/j.watres.2025.120567

[26] Chen, J., & Zhang, L. (2025). Illicit sewage connection fuels CH_4 and CO_2 emissions in storm sewer: Tracking from sources to mechanical influences. *Environmental Science & Technology*, 59(8), 3850–3861. https://doi.org/10.1021/acs.est.4c08765

[27] Kong, Z., Wang, L., & Li, Y. (2023). Status of research on greenhouse gas emissions from wastewater collection systems. *International Journal of Environmental Research and Public Health*, 20(14), 6352. https://doi.org/10.3390/ijerph20146352

[28] Liu, Y., Ni, B. J., & Yuan, Z. (2025). Assessment of methane and nitrous oxide emissions from urban community sewer networks: Field quantification and insights into environmental factors. *Water Research*, 248, 120856. https://doi.org/10.1016/j.watres.2025.120856

[29] Wang, L., Chen, D., & Liu, S. (2024). Intelligent management of carbon emissions of urban domestic sewage based on the Internet of Things. *Environmental Research*, 246, 118025. https://doi.org/10.1016/j.envres.2024.118025